

# Developing a Linear Quadratic Regulator for Human Lower Extremity Exoskeleton Robot

<sup>1</sup>Sk Khairul Hasan and <sup>2</sup>Anoop Dhingra

<sup>1</sup>Department of Mechanical and Manufacturing Engineering, Miami University, USA

<sup>2</sup>Department of Mechanical Engineering, University of Wisconsin Milwaukee, USA

## Article history

Received: 22-03-2022

Revised: 10-04-2022

Accepted: 19-04-2022

## Corresponding Author:

Sk Khairul Hasan  
Department of Mechanical and  
Manufacturing Engineering,  
Miami University, USA  
E-mail: hasansk@miamioh.edu

**Abstract:** During the last two decades, exoskeleton robot-assisted neurorehabilitation has received a lot of attention. The major reason for active research in robot-assisted rehabilitation is its ability to provide various types of physical therapy at different stages of physical and neurological recovery. The performance of the robot-assisted physical therapy is greatly influenced by the robot motion control system. Robot dynamics are nonlinear, but many linear control schemes can adequately handle the nonlinear dynamics with the help of feedback linearization techniques. In this study, the dynamic model of the human lower extremities was developed. A state-space form of the human lower extremity nonlinear dynamic model is presented. LuGre friction model was used to simulate the robot joint friction. A Linear Quadratic Regulator (LQR) was designed to control the human lower extremity dynamics. Dynamic simulations were carried out in the Matlab-Simulink environment. The designed controller's tracking performance was demonstrated in the presence of joint friction. The developed controller's tracking performance is assessed by comparing the results obtained using LQR with other linear and nonlinear controllers (PID, Computed torque control, and Sliding mode control). For performance verification, the same robot dynamics, friction model, and trajectories were used. The stability of the developed control system is also analyzed.

**Keywords:** Exoskeleton Robot, State-Space Modeling, LQR, Lower Extremity Dynamic Model

## Introduction

A full or partial loss of control of the lower extremities is defined as a Human Lower Extremity (HLE) physical disability. This may happen due to neurological injuries, muscular problems, skeletal problems, or because of amputation. The HLE consists of 7 degrees of freedom; single or multiple joint problems, or amputation brings lower extremity disability in a person's life. According to a World Health Organization report, annually, post-stroke, about 10 million people survive with minor to significant impairments. Physical therapy helps in post-stroke recovery. Lower extremity physical disability may also result from spinal cord injuries, trauma, sports injuries, or occupational injuries. Since HLE physical disability affects mobility, it is vital to reduce the disability period as much as possible. Most of the time, the recovery period is prolonged and the recovery performance depends on the competence of the physiotherapist. It's challenging to manage a big number of impaired persons with limited resources. Exoskeleton robot-

assisted physical therapy is a promising alternative to traditional physiotherapy.

Over the last two decades, an enormous amount of research has been conducted on the application of exoskeleton robots in neurorehabilitation (Yan *et al.*, 2015). The main advantages of exoskeleton robot-based neurorehabilitation are: That at any level of physical recuperation, the robot may deliver tailored therapy on an ongoing basis and can effectively assess the patient's healing rate (Meng *et al.*, 2015). Due to the application of the exoskeleton robot, a physiotherapist does not even have to stay with a patient for a substantial period. With the development of haptic devices, a physiotherapist can apply a controlled amount of force/torque to the limb via an exoskeleton robot.

A robot is a high-precision electromechanical system consisting of sensing, computation, and actuation units. Different units communicate amongst themselves by using various standard communication technologies. To achieve maximum efficiency, all units

must be efficient and appropriately synchronized. Due to a lack of appropriate control algorithms, high-performance sensors and actuators may not be able to ensure optimal robot maneuverability.

The sensors attached to the mechanical structures or with the actuators (Fig. 1) measure position, velocity, or acceleration. The high-performance computer executes the governing control algorithms based on the received signals from the sensors and sends actuation commands to the actuator drives. The actuators move mechanical structures.

The accuracy and precision of the robot joint movements determine the efficacy of exoskeleton robot-based physical therapy. An effective control system is essential to run the robot efficiently and deliver different forms of physical therapy smoothly. To achieve this goal, researchers have designed and used many control schemes.

The DoF, sensing, actuation technology, and governing control methodologies of existing human lower extremity exoskeleton robots are summarized in Table 1. Nonlinear robot dynamics have been handled using both linear and nonlinear control techniques. While robot dynamics is nonlinear, it can be linearized and linear control techniques can be applied to control the robot.

The physical dynamics of the human lower extremities are nonlinear. With the help of linearization techniques, linear control techniques can be applied effectively to control nonlinear dynamics. LQR is an optimal control technique that allows the designer to select the state feedback gains systematically. The main advantage of LQR over PD, PID, and pole placement is that it is very challenging to establish the link between pole location and performance index/cost function. LQR provides a systematic way to minimize the cost function (in terms of tracking performance and control effort) while meeting performance specifications.

A study of existing human lower extremity rehabilitation exoskeleton robots indicated that nonlinear robot dynamics are handled using both linear and nonlinear control schemes. The majority of the LQR based control applications focused on self-balancing two-wheel mobile robots (Engin, 2018; Wei and Yao, 2015; Zhao and Ruan, 2008; Morales *et al.*, 2018), or two-link planar robots (Ortega-Vidal *et al.*, 2020; Singh *et al.*, 2010; Schoenwald *et al.*, 1990; Yang *et al.*, 2020; Hazem *et al.*, 2020). It was noticed that there are no reported works that used LQR for controlling a higher degree of freedom (more than 2 DoF) serial link manipulator. Further, there are no comparative studies on the performance of LQR and other linear/nonlinear control schemes.

In this research, a 7 DOF human lower extremity dynamic model is built and the nonlinear dynamic model is linearized using a feedback linearization technique. A state-space model of the system is presented. An LQR is designed to control the HLE dynamics. To simulate joint friction, a LuGre friction model is incorporated into the dynamic model. A comparative study between LQR, PID, Computed Torque Control (CTC) and Sliding Mode Controller (SMC) is presented.

There are seven sections in this study. The anatomy of the HLE is discussed in the second section. Anthropomorphic modeling of the exoskeleton robot requires a thorough understanding of lower extremity anatomy. The HLE's kinematic and dynamic model, as well as joint friction modeling and state-space representation, are described in section three. The LQR controller design technique, as well as the setup of the controller cost function and controller stability analysis, are covered in section four. Section five describes the simulation results obtained using LQR. Section six presents a performance comparison between LQR, PID, Computed torque control, and Sliding mode control techniques. Finally, in section seven, some final remarks on this study are presented.

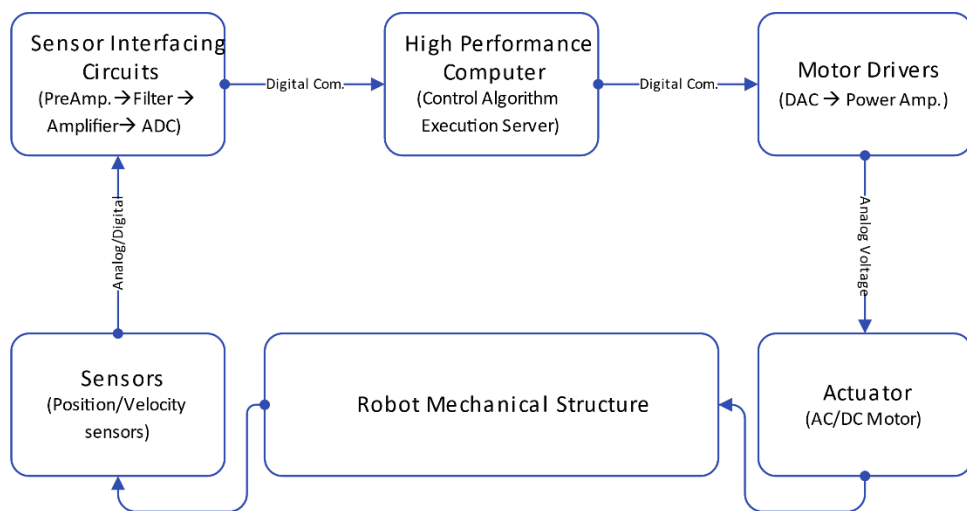


**Fig. 1:** A rehabilitation robot's mechatronics system architecture

**Table:** Existing rehabilitation robots along with their DoF, sensing, actuation, and Control

# Device name	Degrees of freedom	Actuator type	Feedback/ intention sensing method	Control algorithm	Ref.
1. EXPOS And SUBAR	Hip: F-E (A) Knee: F-E (A) Ankle: (U) Double legs	DC motor	Force sensor	Fuzzy logic control, Impedance control	Kyoungchul and Doyoung (2006)
2. Lokomoat	Pelvis: VM (U) Hip: F-E (A) Knee: F-E (A) Ankle: F-E (U) Double legs	DC motor Force sensor	Goniometer, position control	Hybrid force-	Colombo <i>et al.</i> (2000; Bernhardt <i>et al.</i> , 2005)
3. Lopes	Pelvis: L-R, F-B Hip: F-E(A) A-A (A) Knee: F-E (A) Double legs	SEA	Spring-based passive force sensor	Impedance control	Veneman <i>et al.</i> (2007; 2006)
4. ALEX	Trunk: 3 DOF Hip: F-E (A), A-A(U) Knee: F-E (A) Ankle: F-E(U) Single leg	Linear actuator, Spring as a passive actuator	Force and torque sensor	Force, impedance control	Banala <i>et al.</i> (2007; Agrawal <i>et al.</i> , 2007; Kim, 2010; Stegall <i>et al.</i> , 2012)
5. HAL	Hip: F-E (A) Knee: F-E (A) Ankle: F-E (U) Single leg	DC servo motor	sEMG signals	Proportional myoelectric control	Kawamoto and Sankai (2004; Suzuki <i>et al.</i> , 2007; Kawamoto <i>et al.</i> , 2009)
6. REWALK	Hip: F-E(A) Knee: F-E(A) Foot: F-E(U) Double legs	DC motor	Motion sensor, tilt sensor	Proportional myoelectric control	Zelig <i>et al.</i> (2012; Esquenazi <i>et al.</i> , 2012)
7. ELEGS	Hip: A-A (U) F-E (A) Knee: F-E (A) Ankle: F-E (U)	Hydraulic actuator	Switching system	Finite state machine	Strickland (2011)
8. Vanderbilt Exoskeleton	Hip: F-E (A) Knee: F-E (A) Double legs	Electric motor	Using user vocal commands, Center of Pressure triggered	Proportional myoelectric control	Farris <i>et al.</i> (2013)
9. ATLAS	Hip: F-E (A) Knee: F-E (A) Ankle: F-E(U)	Brushless DC motor	Switching via the user interface	Finite state machine /PD control	Sanz-Merodio <i>et al.</i> (2012)
10. MINA	Hip: F-E (A) Knee: F-E (A) Ankle: F-E(U) Double legs	Brushless DC motor	Switching via the user interface	PD control	Neuhaus <i>et al.</i> (2011)
11. Mind walker	Hip: A-A (A) F-E(A) Knee: F-E(A) Ankle: F-E (U) Double legs	SEA compliant actuator, Springs	Switching via the user interface	Model predictive control based gait pattern generation	Wang <i>et al.</i> (2013)
13. Ortholeg and Ortholeg 2.0	Hip: F-E (A) A-A (U) Knee: F-E (A) Ankle: F-E(U) Double Legs	DC motor	Electrooculography and switches	Brain wave control	Araujo <i>et al.</i> (2015); Gloge <i>et al.</i> , 2015)
14. Walking assistance lower limb exoskeleton	Hip: F-E (A) A-A (U) Knee: F-E (A) Ankle: U Double Legs	DC brushless motor	Inclinometer and force sensor	Center of Pressure Control	Kim <i>et al.</i> (2013)
15. IHMC mobility assist exoskeleton	Hip: F-E (A), A-A (A), R-R (U) Knee: F-E (A) Ankle: F-E (U) Double Legs	Rotary series elastic actuator	Optical encoder works as a passive force sensor	Position, force/ torque control	Kwa <i>et al.</i> (2009)

**Table 1:** Continue

16. Lower-limb power assist exoskeleton	Hip: F-E(A) Knee: F-E(A) Ankle: U	BLDC motor based series elastic actuator	Torque sensor	PI velocity control loop nested in a torque control loop	Tagliamonte <i>et al.</i> (2013)
17. WPAL (Wearable Power-Assist Locomotor)	Hip: F-E(A) Knee: F-E(A) Ankle: F-E(A) Double legs	DC servo motor	Encoder and force sensor	Swing phase step trajectory control	Jianfeng <i>et al.</i> (2013)
18. ABLE	Hip: F-E Knee: F-E Ankle: F-E	DC motor	Inclinometer, mechanical and touch switch measurement wheel, load cell, potentiometer	PD control	Mori <i>et al.</i> (2006)
19. Body Extender	12 DoF for both legs	PM DC motor	Force sensor, Accelerometer	-	Marcheschi <i>et al.</i> (2011)
20. Nurse robot suit	Supports shoulder, waist, legs	Micro air pump for rotating .pneumatic actuators	Pressure sensor, Muscle hardness sensor	PID control	Yoshimitsu and Yamamoto (2004; Yamamoto <i>et al.</i> , 2004)
24. Barkeley Exoskeleton System	Hip: F-E (A), A-A (A), R (U) Knee: F-E (A) Ankle: A-A(U), F-E(A) R, Toe: F-E	Hydraulic piston cylinder	Force sensor, encoder	Force position hybrid controller	Zoss <i>et al.</i> (2006; Kazerooni <i>et al.</i> , 2006)
25. CUHK-Exo	Hip: F-E (A), R Knee: F-E (A) Ankle: F-E(P)	DC motor	Encoder, potentiometer, Inertia measurement unit, Force-sensitive resistor, mechanical switch	PD controller	Chen <i>et al.</i> (2017); Chen <i>et al.</i> , 2019)

## Anatomical Features of Human Lower Extremity

Understanding the degrees of freedom, ranges of motion and inertial properties of the lower extremities requires knowledge of HLE anatomy. The degrees of freedom, range of motion, and anthropometric factors that were used to construct a dynamic model of the robot are outlined next.

### Degrees of Freedom at the Human Lower Extremities

There are seven degrees of freedom in the human lower extremity. The bones and joints of the human lower extremity are depicted in 81B Fig. 2. A three-degree-of-freedom ball-and-socket joint connects the femur to the pelvis, allowing rotation around 3 independent axes:

1. Hip abduction adduction
2. Hip flexion-extension
3. Hip internal and external rotation

The femur is joined to the tibia and fibula in the knee joint by the femoral condyle. Russell *et al.* (2018) described the shape and size of the femoral condyle, as well as its instantaneous center of rotation. The elliptical contact surface generates both rotational and linear displacement in the knee joint. During flexion, the leg length increases, while during extension, it decreases (Hasan *et al.*, 2020). The DOF of the human lower extremities is shown in Fig. 3.

The knee joint provides 2 DOF that correspond to

1. Knee flexion and extension
2. Shank internal and external rotation

Two degrees of freedom are provided by the tibia and fibula, which are linked to the talus at their lower ends. The following motions are permitted:

1. Ankle flexion-extension
2. Ankle pronation and supination

### Ranges of Motion of the Human Lower Extremity

The range of motion of the exoskeleton robot joints must be established considering human lower extremity ranges of motion. The range of motion of lower extremity joints for healthy people is similar. The permitted range values in physical therapy vary depending on the health status of the individual patient. The reported human lower extremity ranges of motion from a variety of sources are shown in Table 1. In this study, Kurz's range of motion is employed to produce the full range of motion trajectories.

### Anthropometric Parameters

The design of kinematic and dynamic models of the human lower extremity requires an understanding of anthropometrical features. Based on data from 5290 individuals, Nikolova and Toshev studied the anthropometrical features (2435 males and 2855 females). In 2008, they published the findings of their research (Nikolova and Toshev, 2008).

Contini (1972) provided several empirical equations for determining anthropometrical parameters of the human lower extremity depending on the subject's weight and height. The lower extremity anthropometrical properties are calculated using the following empirical equations:

$$B_d = 0.6905 + 0.0297C \frac{lb}{ft^3}, \text{ where } C = HW^{-\frac{1}{3}} \quad (1)$$

In Eq. (1)  $B_d$  presents the body density ( $lbs/ft^3$ ),  $H$  presents the height of the subject (inch), and  $W$  is the bodyweight of the subject ( $lbs$ ). The following formulae ((2)-(4)) determine the densities of the thigh, shank, and foot:

$$T_d = 1.035 + 0.814 * B_d \frac{lb}{ft^3} \quad (2)$$

$$S_d = 1.065 + B_d \frac{lb}{ft^3} \quad (3)$$

$$F_d = 1.071 + B_d \frac{lb}{ft^3} \quad (4)$$

Using bodyweight and density, the whole-body volume ( $B_v$ ) was computed:

$$B_v = \frac{W}{B_d} ft^3 \quad (5)$$

The following formula ((6)-(8)) were used to compute the volume of the thigh, shank, and foot:

$$T_v = 0.0922 * B_v ft^3 \quad (6)$$

$$S_v = 0.0464 * B_v ft^3 \quad (7)$$

$$F_v = 0.0124 * B_v ft^3 \quad (8)$$

The Eq. (9)-(11) were used to calculate the weights of the thigh, shank, and foot:

$$T_m = T_v * T_d lbs \quad (9)$$

$$S_m = S_v * S_d lbs \quad (10)$$

$$F_m = F_v * F_d lbs \quad (11)$$

Equation (12)-(15) determined the length of the thigh ( $T_l$ ), shank ( $S_l$ ) foot ( $F_l$ ), and ankle to the lower face of the foot ( $A_g$ ). The length of the thigh ( $T_l$ ), shank ( $S_l$ ), foot ( $F_l$ ), and from the ankle to the foot's lower surface ( $A_g$ ) Eq. (12)-(15) were used to calculate the values:

$$T_l = 0.245 * H \text{ inch}, \quad (12)$$

$$S_l = 0.285 * H \text{ inch}, \quad (13)$$

$$F_l = 0.152 * H \text{ inch}, \quad (14)$$

$$A_g = 0.043 * H \text{ inch} \quad (15)$$

Equation (16)- (18),  $T_{cm}$ ,  $S_{cm}$  and  $F_{cm}$  give the locations of the center of mass from the proximal joint (for thigh ( $T_{cm}$ ), shank ( $S_{cm}$ ) and foot ( $F_{cm}$ )):

$$T_{cm} = 0.41 * T_l \text{ inch}, \quad (16)$$

$$S_{cm} = 0.393 * S_l \text{ inch}, \quad (17)$$

$$F_{cm} = 0.445 * F_l \text{ inch} \quad (18)$$

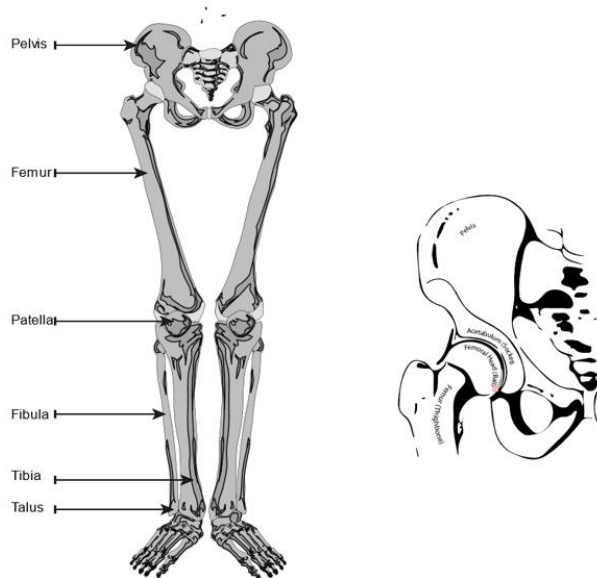


**Fig. 2:** Left: Bones and joints of the human lower extremity, right: Ball and socket joint between the pelvis and hip

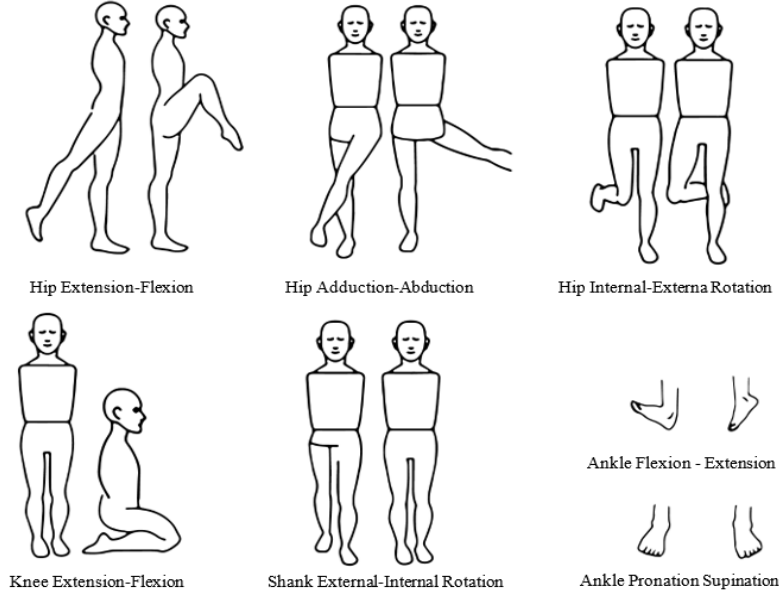


**Fig. 3:** Degrees of freedom in human lower extremities

The empirical equations for the inertial properties of the thigh  $T_i$ , shank  $S_i$ , and foot  $F_i$  are given in empirical Eq. (19)-(21), describe the inertial characteristics of the thigh  $T_i$ , shank  $S_i$ , and foot  $F_i$ :

$$T_i = \begin{bmatrix} T_m(0.124*T_l)^2 & 0 & 0 \\ 0 & T_m(0.267*T_l)^2 & 0 \\ 0 & 0 & T_m(0.267*T_l)^2 \end{bmatrix} \quad (19)$$

$$S_i = \begin{bmatrix} S_m(0.281*S_l)^2 & 0 & 0 \\ 0 & S_m(0.114*S_l)^2 & 0 \\ 0 & 0 & S_m(0.275*S_l)^2 \end{bmatrix} \quad (20)$$

$$F_i = \begin{bmatrix} F_m(0.124*F_l)^2 & 0 & 0 \\ 0 & F_m(0.245*F_l)^2 & 0 \\ 0 & 0 & F_m(0.257*F_l)^2 \end{bmatrix} \quad (21)$$

### Kinematic and Dynamic Modeling of the Human Lower Extremity

From the standpoint of control, developing a dynamic model of a robot is fundamental. It is quite impossible to develop and realize the controller without dynamic simulation. An unstable controller can damage the robot and lead to disaster. It is crucial to simulate the robot's dynamic model, which includes the controller, and then test it on the hardware level. The HLE kinematic and dynamic modeling, friction modeling, and state-space presentation of the dynamic model of the human lower extremity will be explained in the following paragraphs.

### *Kinematic and Dynamic Modeling of the Lower Extremities*

The kinematic model was developed using a modified Denavit-Hartenberg (DH) parameters technique (Craig, 2005). Each degree of freedom had its own set of link frames. The link frame are assigned based on the modified DH parameter (Fig. 4 and 5)

The transformation matrix's general form is given in Eq. (22):

$${}^{i-1}T = \begin{bmatrix} \cos\theta_i & -\sin\theta_i & 0 & \alpha_{i-1} \\ \sin\theta_i \cos\alpha_{i-1} & \cos\theta_i \cos\alpha_{i-1} & -\sin\alpha_{i-1} & -\sin\alpha_{i-1}d_i \\ \sin\theta_i \sin\alpha_{i-1} & \cos\theta_i \sin\alpha_{i-1} & \cos\alpha_{i-1} & \cos\alpha_{i-1}d_i \\ 0 & 0 & 0 & 1 \end{bmatrix} \quad (22)$$

The transformation matrices Eq. (23) to (29) were found by substituting the values of modified DH parameters from Table 3 into Eq. (22):

$${}^0T_1 = \begin{bmatrix} \cos(\theta_1) & -\sin(\theta_1) & 0 & 0 \\ \sin(\theta_1) & \cos(\theta_1) & 0 & 0 \\ 0 & 0 & 1 & 0 \\ 0 & 0 & 0 & 1 \end{bmatrix} \quad (23)$$

$${}^1T_2 = \begin{bmatrix} \sin(\theta_2) & \cos(\theta_2) & 0 & 0 \\ 0 & 0 & 1 & 0 \\ \cos(\theta_2) & -\sin(\theta_2) & 0 & 0 \\ 0 & 0 & 0 & 1 \end{bmatrix} \quad (24)$$

$${}^2T_3 = \begin{bmatrix} \cos(\theta_3) & -\sin(\theta_3) & 0 & 0 \\ 0 & 0 & 0 & -l_1 \\ -\sin(\theta_3) & -\cos(\theta_3) & 1 & 0 \\ 0 & 0 & 0 & 1 \end{bmatrix} \quad (25)$$

$${}^3T_4 = \begin{bmatrix} \cos(\theta_4) & -\sin(\theta_4) & 0 & 0 \\ 0 & 0 & -1 & 0 \\ \sin(\theta_4) & \cos(\theta_4) & 0 & 0 \\ 0 & 0 & 0 & 1 \end{bmatrix} \quad (26)$$

$${}^4T_5 = \begin{bmatrix} \cos(\theta_5) & -\sin(\theta_5) & 0 & 0 \\ 0 & 0 & 1 & -l_2 \\ -\sin(\theta_5) & -\cos(\theta_5) & 0 & 0 \\ 0 & 0 & 0 & 1 \end{bmatrix} \quad (27)$$

$${}^5T_6 = \begin{bmatrix} \sin\sin(\theta_6) & \cos\cos(\theta_6) & 0 & 0 \\ 0 & 0 & -1 & 0 \\ -\cos\cos(\theta_6) & \sin\sin(\theta_6) & 0 & 0 \\ 0 & 0 & 0 & 1 \end{bmatrix} \quad (28)$$

$${}^6T_7 = \begin{bmatrix} \cos(\theta_7) & -\sin(\theta_7) & 0 & a_1 \\ 0 & 0 & 1 & 0 \\ -\sin(\theta_7) & -\cos(\theta_7) & 0 & 0 \\ 0 & 0 & 0 & 1 \end{bmatrix} \quad (29)$$

The homogeneous transformation matrix defines the location and orientation of the end frame concerning the base frame. In this case, it refers to the location and orientation of the foot relative to the hip. Individual transformation matrices from Eq. (23) through Eq. (29) were multiplied together to generate the homogeneous transformation matrix:

$${}^0T_7 = \begin{bmatrix} 0 & 1 & 2 & T_3 & T_4 & T_5 & T_6 & T_7 \\ T_1 & T_2 & T_3 & T_4 & T_5 & T_6 & T_7 & 1 \end{bmatrix} \quad (30)$$

The Newton-Euler law is a well-known mathematical procedure for expressing dynamic equations of motion of a serial link manipulator. Presented next is an explanation of the Newton-Euler formulation.

**Table 2: Human lower extremity ranges of motion**

Joint	Movement	American Academy of orthopedic Surgeons (1965)	Kendall and McCarry (2005)	American Medical Association	Kurz (2015)
Hip					
Flexion	0-120°	0-125°	0-100°	0-130°	
Extension	0-30°	0-10°	0-30°	0-130°	
Abduction	0-45°	0-45°	0-40°	0-50°	
Adduction	0-30°	0-10°	0-20°	0-30°	
Internal Rotation	0-45°	0-45°	0-40°	0-40°	
External Rotation	0-45°	0-45°	0-50°	0-45°	
Knee					
Flexion	0-135°	0-140°	0-150°	0-130°	
Extension	-	-	-	0-15°	
Internal Rotation	-	-	-	0-10°	
External Rotation	-	-	-	0°	
Ankle					
Dorsiflexion	0-20°	0-20°	0-20°	0-20°	
Plantar flexion	0-50°	0-45°	0-40°	0-45°	
Inversion/Pronation	0-350°	0-35°	0-30°	0-30°	
Eversion/Supination	0-15°	0-20°	0-20°	0-20°	

For a moving link, Newton's equation of motion is:

$$F = m\ddot{v}_c \quad (31)$$

where,  $F$  is the external force,  $m$  is the mass of the link and  $\ddot{v}_c$  is the acceleration at the link's center of mass. Euler's equation of motion is given as:

$$N = {}^cI_{\dot{\omega}} + \omega \times {}^cI_{\omega} \quad (32)$$

where,  $N$  is the torque operating at the link's center of mass and  ${}^cI$  is the inertia tensor at the link's center of mass. Here  $\omega$  and  $\dot{\omega}$  are the angular velocity and acceleration of the link at its mass's center. There are two phases in the Newton-Euler formulation.

#### Phase I: Outward Iteration to Compute Velocity and Acceleration Propagation

The first phase involves iteratively propagating angular velocity  $\omega$  and angular acceleration  $\dot{\omega}$  from link 1 to link  $n$ . Eq. (33) and (34) describe the angular velocity ( $\omega$ ) and angular acceleration ( $\dot{\omega}$ ) propagation from one link to the next:

$${}^{i+1}\omega_{i+1} = {}^{i+1}R {}^i\omega_i + \dot{\theta}_{i+1} {}^{i+1}\hat{Z}_{i+1} \quad (33)$$

$${}^{i+1}\dot{\omega}_{i+1} = {}^{i+1}R {}^i\dot{\omega}_i + {}^{i+1}R {}^i\omega_i \times \dot{\theta}_{i+1} {}^{i+1}\hat{Z}_{i+1} + \ddot{\theta}_{i+1} {}^{i+1}\hat{Z}_{i+1} \quad (34)$$

Eq. (35) to Eq. (36) describes the linear acceleration propagation from the link frame to the center of mass of the link:

$${}^{i+1}\dot{v}_{i+1} = {}^{i+1}R \left[ {}^i\dot{\omega}_i \times {}^iP_{i+1} + {}^i\omega_i \times ( {}^i\omega_i \times {}^iP_{i+1} ) + {}^i\dot{v}_i \right] \quad (35)$$

$${}^i\dot{v}_{ci} = {}^i\dot{\omega}_i \times {}^iP_{ci} + {}^i\omega_i \times ( {}^i\omega_i \times {}^iP_{ci} + {}^i\dot{v}_i ) \quad (36)$$

**Table 3:** Human lower extremity modified D-H parameters

Joint name	Joint variable	Link offset	Link length	Link twist
	$\theta_i$	$d_i$	$a_{(i-1)}$	$\alpha_{(i-1)}$
Hip abduction/adduction	$q_1$	0	0	0
Hip flexion/extension	$q_2 - \frac{\pi}{2}$	0	0	$-\frac{\pi}{2}$
Hip internal/external rotation	$q_3$	$-l_1$	0	$-\frac{\pi}{2}$
Knee flexion/extension	$q_4$	0	0	$\frac{\pi}{2}$
Knee internal rotation	$q_5$	$-l_2$	0	$-\frac{\pi}{2}$
Ankle dorsiflexion/plantarflexion	$q_6 - \frac{\pi}{2}$	0	0	$\frac{\pi}{2}$
Ankle pronation/supination	$q_7$	0	$a_1$	$-\frac{\pi}{2}$

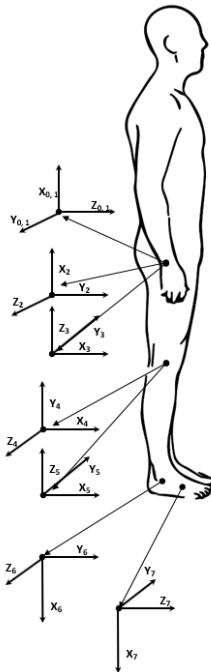


**Fig. 4:** Assigning Link Frames Using a Modified D-H Parameter

Equation (37) and (38) can be used to compute force and torque acting on the center of mass of the link:

$${}^{i+1}F_{i+1} = m_{i+1} {}^{i+1}\dot{v}_{i+1} \quad (37)$$

$${}^{i+1}N_{i+1} = {}^{c_{i+1}}I_{i+1} {}^{i+1}\dot{\omega}_{i+1} + {}^{i+1}\omega_{i+1} \times {}^{c_{i+1}}I_{i+1} {}^{i+1}\omega_{i+1} \quad (38)$$

#### Phase II: Inward Iteration is used to Calculate the Propagation of Forces and Torques

The forces and torques transmitted to the base frame from the end effector are calculated during the inward iteration. Equation (39)-(41) are used to calculate the force and torque propagation. A more detailed explanation of this phase can be found in (Craig, 2005):

$${}^i f_i = {}_{i+1}{}^i R {}^{i+1} f_{i+1} + {}^i F_i \quad (39)$$

$${}^i n_i = {}^i N_i + {}_{i+1}{}^i R {}^{i+1} n_{i+1} + {}^i P_c \times {}^i F_i + {}^i P_{i+1} \times {}_{i+1}{}^i R {}^{i+1} f_{i+1} \quad (40)$$

$$\tau_i = {}^i n_i^T {}^i \hat{Z}_i \quad (41)$$

The joint torques are obtained by equating the  $\hat{Z}$  component of the torque ( ${}^i n_i$ ) in Eq. (41).

The dynamic equation of motion of the robot is given by Eq. (42):

$$\tau_{Joint} = \left[ M(\theta) \ddot{\theta} + V(\theta, \dot{\theta}) + G(\theta) \right] \quad (42)$$

In Eq. (43),  $M(\theta)$ ,  $(7 \times 7)$  is known as the mass matrix, ( $M$  is a symmetric positive definite matrix),  $V(\theta, \dot{\theta})$ ,  $(7 \times 1)$  matrix presents the Coriolis and the centripetal term and  $G(\theta)$ ,  $(7 \times 1)$  matrix presents the gravitational force.  $\tau_{Joint}$ ,  $(7 \times 1)$  matrix presents the joints torque requirements for tracing the trajectory. Equation (43) can be used to represent the robot's dynamical equation of motion:

$$\ddot{\theta} = M(\theta)^{-1} \left[ \tau_{Joint} - V(\theta, \dot{\theta}) - G(\theta) \right] \quad (43)$$

$M(\theta)^{-1}$  always exists because  $M(\theta)$  is a positive definite matrix. The ideal/model robot dynamics are schematically presented in Fig. 6. Joint friction was not taken into account in the ideal case.

#### Friction Modeling

Bearings, transmission, and seals connect links in a robotic manipulator. Friction forces or torques are created at the joint due to relative motion between contact surfaces. The friction force (or torque) has been estimated up to 50% of the transmitted force or torque (Liu and

Chen, 2019). To compensate for the influence of friction, robustness is required in a robot control system. Numerous factors influence the amount of friction force or torque generated, including contact surface roughness, lubricant viscosity, transmitted load, temperature, the relative velocity between two contact surfaces, and so on. The majority of friction-related characteristics are variable. It's tough to distinguish between the effects of different parameters making it nearly impossible to create a theoretical model of friction phenomena. Most friction models developed are empirical and have been used successfully for many years. To explain the friction phenomena, various theories have been presented, including the Coulomb friction model, viscous friction model, Stribeck effect, pre-sliding behavior, tiny displacement in the stiction phase, hysteretic effect, and others. There are advanced friction models available, such as the Dahl, LuGre, and Karnopp models (Ha *et al.*, 2006).

The application determines which friction model to use. In this study, the LuGre friction model is used (Ha *et al.*, 2006) and is based on the summation of the Coulomb friction model, the Viscous friction model, and the Stribeck effect. The friction model utilized in this study will be briefly explained in the next paragraph.

**The Coulomb friction ( $T_c$ ):** According to the Coulomb friction model, friction torque is a constant number at all times.

**The viscous friction ( $T_v$ ):** Produces a resistive torque proportional to the contact surfaces' relative velocity.

**The Stribeck friction ( $T_s$ ):** At low velocities, the Stribeck effect simulates negatively sloping features.

The combined friction model is presented in Eq. (44). The friction torque is calculated using Eq. (44) to (46):

$$T = \sqrt{(2e)}(T_{brk} - T_c) \cdot \exp\left(-\left(\frac{\omega}{\omega_{St}}\right)^2\right) + \frac{\omega}{\omega_{St}} + T_c \cdot \tanh\left(\frac{\omega}{\omega_{Coul}}\right) + f\omega \quad (44)$$

$$\omega_{St} = \omega_{brk} \sqrt{2} \quad (45)$$

$$\omega_{Coul} = \frac{\omega_{brk}}{10} \quad (46)$$

where:

$T$  = The overall friction torque

$T_c$  = Presents the Coulomb friction torque

$T_{brk}$  = The breakaway friction torque: The breakaway friction is computed as the total of the Coulomb and Stribeck friction torques in the vicinity of zero velocity.

$\omega_{brk}$  = The breakaway friction velocity: The maximum velocity at which the Stribeck friction occurs. The

breakaway friction torque is equal to the sum of the Stribeck and Coulomb friction at this point.

$\omega_{St}$  = The Stribeck velocity threshold

$\omega_{Coul}$  = The Coulomb velocity threshold

$\omega$  = The input angular velocity

$F$  = The coefficient of viscous friction: The friction torque and the rotational velocity have a proportionality coefficient.

The value of the parameter must be positive.

Figure 7 presents the relation between the angular velocity and friction torque in the friction model.

Figure 8 shows the friction torque simulation using Eq. (44) to (46)

The following parameter values were used in the simulation above:

$$T_{peak} = 100 \text{ Nm}, \omega = 100 \text{ rad/sec}, f = 5 \text{ Nm/(rad/sec)}, \\ T_c = 0.1T_{peak} \text{ Nm}, \omega_{brk} = 0.01 \text{ rad/sec}, T_{brk} = 0.15 T_{peak} \text{ Nm}$$

where relative motion exists, it is impossible to eliminate friction between two mating parts. The robot dynamics get more complex once the joint friction torques are taken into account:

$$\tau_{Joint} = M(\theta)\ddot{\theta} + V(\theta, \dot{\theta}) + G(\theta) + \tau_{friction} \quad (47)$$

where:

$$\tau_{friction} = F(\dot{\theta}) \quad (48)$$

Equation (47) can be written in the form of Eq. (49):

$$\ddot{\theta} = M(\theta)^{-1} [\tau - V(\theta, \dot{\theta}) - G(\theta) - F(\dot{\theta})] \quad (49)$$

The schematic model of the robot dynamics with frictional disturbances is shown in Fig. 9.

### State Space Modeling of the Robot Dynamics

Equation (50) can be used to present the robot dynamics with joint friction:

$$\ddot{\theta} = M(\theta)^{-1} [\tau - V(\theta, \dot{\theta}) - G(\theta) - F(\dot{\theta})] \quad (50)$$

Now, defining the state vector:

$$X = \begin{bmatrix} x_1 \\ x_2 \end{bmatrix} = \begin{bmatrix} \theta \\ \dot{\theta} \end{bmatrix} \quad (51)$$

The resultant state equations are based on Eq. (50) becomes:

$$\dot{x}_1 = \dot{\theta} = x_2 \quad (52)$$

$$B = \begin{bmatrix} 0 \\ I \end{bmatrix} \in \mathbb{R}^{14 \times 7}$$

$$\dot{x}_2 = \ddot{\theta} = M^{-1}(\theta)[\tau - V(\theta, \dot{\theta}) - G(\theta) - F(\dot{\theta})] \quad (53)$$

$$C = [I] \in \mathbb{R}^{14 \times 14}$$

$$= -M^{-1}(x_1)[V(x_1, x_2) + G(x_1) + F(x_2)] + M^{-1}(x_1)\tau \quad (54)$$

$$D = [0] \in \mathbb{R}^{14 \times 7}$$

$$= f(x) + g(x)\tau \quad (55)$$

$$U = f(x) + g(x)\tau \quad (62)$$

where:

$$f(x) = -M^{-1}(x_1)[V(x_1, x_2) + G(x_1) + F(x_2)] \quad (56)$$

$$g(x) = M^{-1}(x_1) \quad (57)$$

The control law:

$$\tau = g^{-1}(x)[-f(x) + u] \quad (58)$$

The equation's state-space form can be written as:

$$\begin{aligned} \dot{x}_1 &= x_2 \\ \dot{x}_2 &= u \end{aligned} \quad (59)$$

$$\begin{bmatrix} \dot{x}_1 \\ \dot{x}_2 \end{bmatrix} = \begin{bmatrix} 0 & I \\ 0 & 0 \end{bmatrix} \begin{bmatrix} x_1 \\ x_2 \end{bmatrix} + \begin{bmatrix} 0 \\ I \end{bmatrix} u \quad (60)$$

$$\dot{X} = AX + Bu \quad (61)$$

$$Y = CX + Du$$

where,  $X \in \mathbb{R}^{14 \times 1}$  The first 7 states represent joint positions, whereas the following 7 states represent joint velocities:

$$A = \begin{bmatrix} 0 & I \\ 0 & 0 \end{bmatrix} \in \mathbb{R}^{14 \times 14}$$

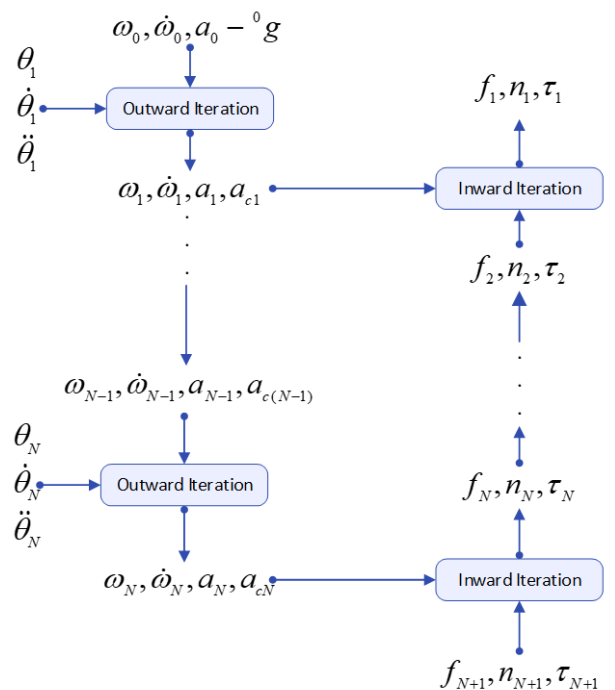


**Fig. 5:** Steps in newton Euler's dynamic equation of motion

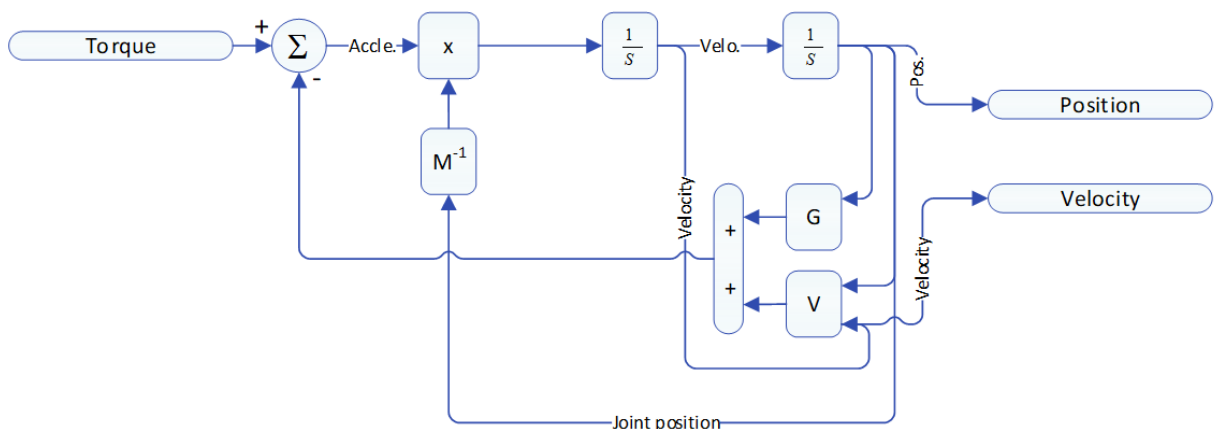


**Fig. 6:** The robot model's internal architecture

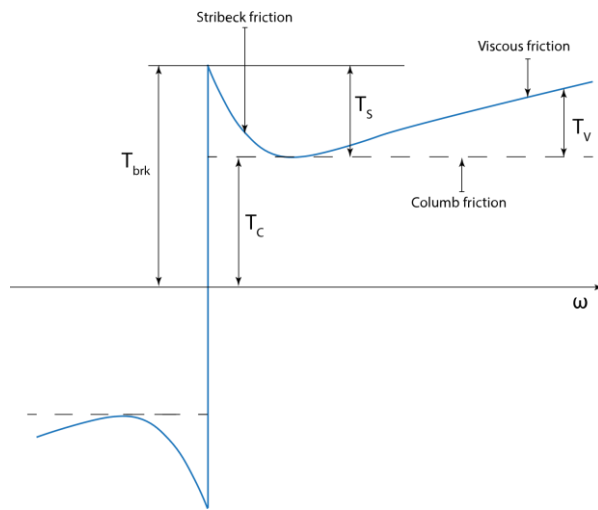


**Fig. 7:** Combined action of the coulomb, viscous, and stribbeck effects

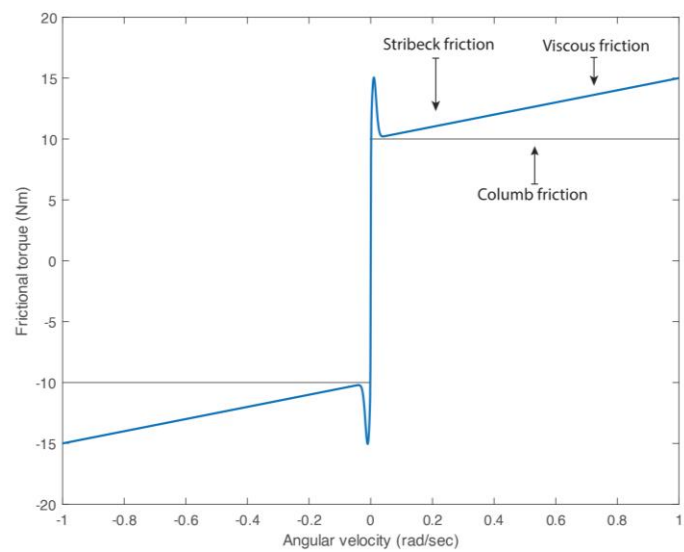


**Fig. 8:** Friction model simulation

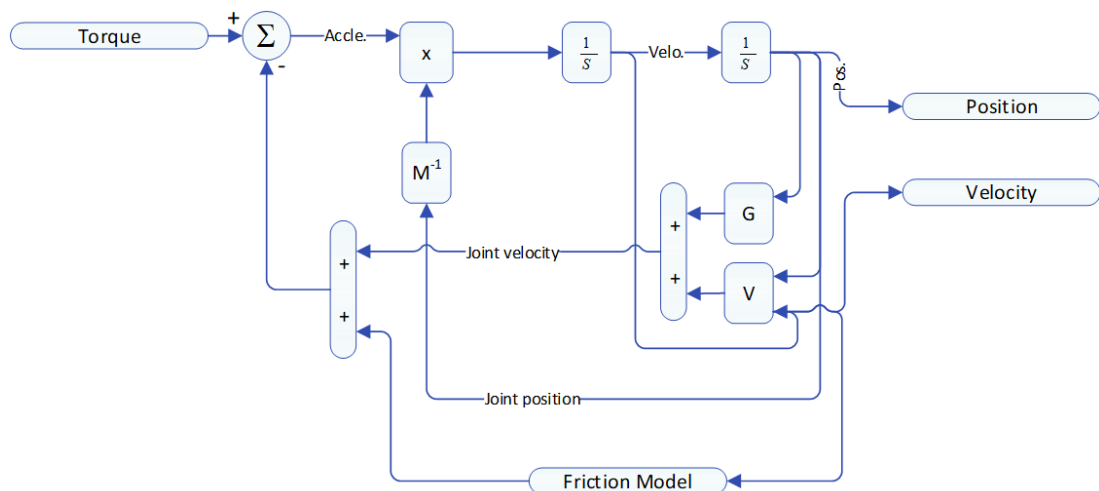


**Fig. 9:** The physical robot model's internal architecture

**Table 4:** Simulation parameters for the HLE dynamic control using LQR

Subject mass	163 lb (73.95 kg)	Distance between → proximal joint and → the center of mass →	Thigh	6.69 in (170 cm)
Subject height	67 in (170.18 cm)		Shank	7.48 in (18.92 cm)
Thigh Mass	12.45 lb (5.65 kg)		Foot	4.5 in (11.5 cm)
Shank mass	7.67 lb (3.48 kg)			
Foot Mass	2.05 lb (0.93 kg)	Thigh inertia g.cm <sup>2</sup> (kg.m <sup>2</sup> )	151 × 10 <sup>3</sup> (0.0151)	0
Thigh-length	16.14 in (41 cm)		0	700 × 10 <sup>3</sup> (0.070)
Shank length	18.89 in (48.79 cm)		0	0
Foot length	10.23 in (25.88 cm)	Shank inertia g.cm <sup>2</sup> (kg.m <sup>2</sup> )	648 × 10 <sup>3</sup> (0.0648)	700 × 10 <sup>3</sup> (0.070)
			0	0
			0	107 × 10 <sup>3</sup> (0.0107)
			0	0
		Foot inertia g.cm <sup>2</sup> (kg.m <sup>2</sup> )	10 × 10 <sup>3</sup> (0.001)	620 × 10 <sup>3</sup> (0.0620)
			0	37 × 10 <sup>3</sup> (0.0037)
			0	0
			0	41 × 10 <sup>3</sup> (0.0041)

## Linear Quadratic Regulator Control Scheme

The Linear Quadratic Regulator (LQR) is characterized as a control law that minimizes a cost function. A cost function is a real nonnegative quantitative measure of the performance of the control system. The LQR controller minimizes the quadratic cost function while achieving the control goals. Frequently, for a robot used in a tracking application, The control law's goal is to reduce tracking error to zero. This is the best decision from a tracking performance perspective, but to reduce the tracking error to zero requires a large control effort (physically, a large control effort means more power expenditures). In reality, for most control applications, the tracking error need not be zero. The role of a control engineer is to achieve a suitable tradeoff between acceptable tracking error and minimum control effort.

For this reason, typically, both tracking error and control effort is included in the cost function:

$$J = \int_0^{\infty} (e(t)^T Q e(t) + u^T R u) dt \quad (63)$$

The relative importance of error  $e(t)$  and the control effort  $u(t)$  is expressed with the help of  $Q$  and  $R$  matrices.

LQR is a linear control scheme, but it can be used for controlling a highly nonlinear system like a robot with the help of the feedback linearization technique. Gravitational force and Coriolis and centrifugal force introduce nonlinearities into robot dynamics. The joint torques required to compensate for the gravitational force and Coriolis and centrifugal force are fed back to linearize the robot dynamic model. For the robotics application, the LQR is developed in two steps. In the first step, the control input  $u(t)$  is determined for the linear model presented in Eq. (60) and then interpret  $u(t)$ , in terms of  $\tau(t)$  by using Eq. (58). Eq. (58) also linearizes nonlinear dynamics by providing additional torque required for linearizing the plant (against gravity, Coriolis, and centrifugal forces), often called feedback linearization.

Consider, at any instant the desired trajectory of the robot is given by  $\theta_d(t), \dot{\theta}_d(t), \ddot{\theta}_d(t)$  and the robot's actual joint position, velocity, and acceleration are given by  $\theta(t), \dot{\theta}(t)$  and  $\ddot{\theta}(t)$

The tracking error is defined as:

$$e(t) = \theta_d(t) - \theta(t) \quad (64)$$

$$\dot{e}(t) = \dot{\theta}_d(t) - \dot{\theta}(t) \quad (65)$$

$$\ddot{e}(t) = \ddot{\theta}_d(t) - \ddot{\theta}(t) \quad (66)$$

Now by defining:

$$\tilde{x}_1 = e \text{ and } \tilde{x}_2 = \dot{e} \quad (67)$$

The robot dynamics Eq. (61) can be rewritten in the form of error dynamics:

$$\dot{\tilde{x}}_1 = \tilde{x}_2 \quad (68)$$

$$\dot{\tilde{x}}_2 = [\ddot{\theta}_d - \ddot{\theta}] \quad (69)$$

$$\dot{\tilde{x}}_2 = \ddot{\theta}_d + M^{-1}(\theta) [V(\theta, \dot{\theta}) + G(\theta) + F(\dot{\theta})] - M^{-1}(\theta) \tau \quad (70)$$

$$\dot{\tilde{x}}_2 = \ddot{\theta}_d + M^{-1}(x_1) [V(x_1, x_2) + G(x_1) + F(x_2)] - M^{-1}(x_1) \tau \quad (71)$$

$$\dot{\tilde{x}}_2 = \ddot{\theta}_d - f(x) - g(x) \tau \quad (72)$$

The control law becomes:

$$\tau = g^{-1}(x) [-f(x) - u + \dot{\theta}_d] \quad (73)$$

Figure 10 shows the control architecture of the Linear Quadratic Controller.

A linear quadratic regulator was designed to get feedback control  $u(t)$  that stabilizes tracking error.

Equation (76) defines the cost function.  $Q \in \mathbb{R}^{14 \times 14}$  and  $R \in \mathbb{R}^{7 \times 7}$  are diagonal matrices given in Eq. (77). From the nature of Q and R matrices, it is visible that to achieve high speed and accuracy the joints angle error  $\tilde{x}$  penalizes much more strongly than control inputs.

The S matrix in Eq. (74) is determined by solving Algebraic Riccati Equation (ARE). With the help of S feedback gain matrix, K was calculated. K always comes with multiple values; only one of them makes the system stable. The closed-loop system's stability may be determined by checking the system's closed-loop pole location using Eq. (78):

$$A^T S + S A - S B R^{-1} B^T S + Q = 0 \quad (74)$$

$$K = R^{-1} B^T S \quad (75)$$

$$J = \int_0^\infty (\tilde{x}^T Q \tilde{x} + u^T R u) dt \quad (76)$$

$$Q = \text{diag} \left\{ 1000, 1000, 1000, 1000, 1000, 1000, 100, 10, 10, 10, 10, 10, 10 \right\} \quad (77)$$

$$R = \text{diag} \left\{ (0.25, 0.25, 0.25, 0.25, 0.25, 0.25, 0.25) \times 10^{-5} \right\},$$

$$\lambda = \text{Eigenvalue}(A - B * K) \quad (78)$$

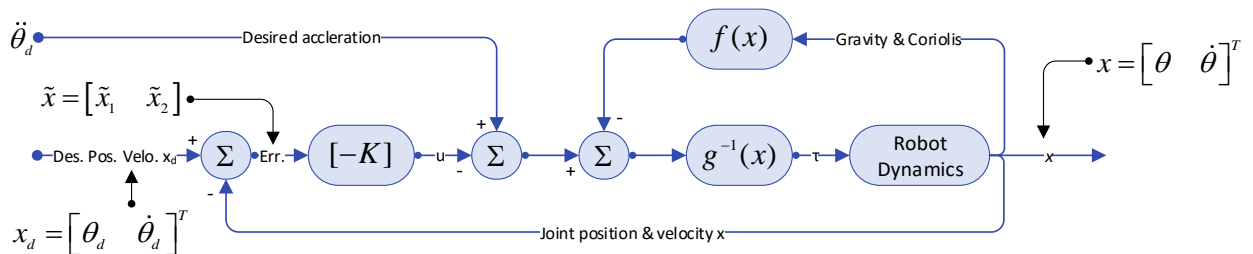


**Fig. 10:** Linear Quadratic Regulator (LQR) controller

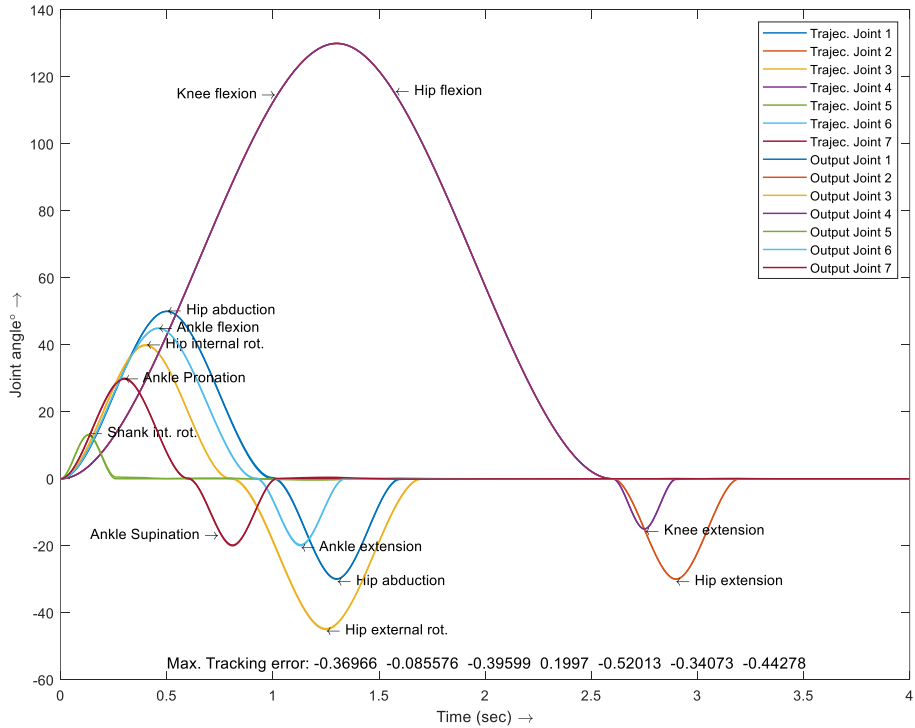


**Fig. 11:** Trajectory tracking performance using LQR

The feedback control law is of the form:

$$U = -K_1 \tilde{x}_1 - K_2 \tilde{x}_2 - \dots - K_7 \tilde{x}_7 \quad (79)$$

where:

$$K_1 = [K_{11} \ K_{12} \ \dots \ K_{17}] \quad (80)$$

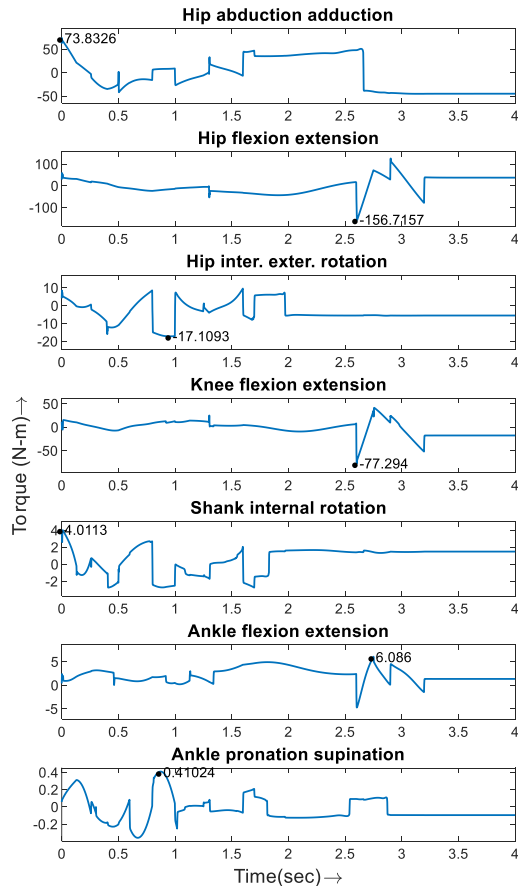
The input torque of the robot becomes:

$$\tau = g^{-1}(x) [-f(x) + K_1 \tilde{x}_1 + K_2 \tilde{x}_2 + \dots + K_7 \tilde{x}_7 + \ddot{\theta}_d] \quad (81)$$

## Simulation Results and Discussion

The Matlab-Simulink® environment was used to execute the simulation. Table 4 shows the mass and inertial properties of the human lower extremities employed in the simulation. The simulation was done for simultaneous joint movements. Figure 11 to 14 show the simulation results using LQR in the presence of joint friction. Table 4 summarizes the parameters used during dynamic simulation.

The parameters used for dynamic friction modeling are given below:



$$\begin{aligned}
 f &= 0.1 \text{ Nm} / (\text{rad/sec}), \tau_{coulamb} \\
 &= 0.1 * \tau_{peak} \text{ Nm}, \tau_{brake} = 0.15 * \tau_{peak} \text{ Nm}, \omega_{strike} \\
 \sqrt{2} \omega_{brake} \text{ rad/sec}, \omega_{coulamb} &= 0.10 * \omega_{brake} \text{ rad/sec}
 \end{aligned}$$

The torque required to track the same trajectory without friction was used to determine all of the peak torques.

The trajectory tracking performance, tracking error, joint torque, and friction torque produced during joint movement is depicted in Figure 11 to 14. From Fig. 11 it can be seen that the maximum tracking error for the simultaneous joint movement was [-0.369°, -0.085°, -0.395°, 0.200°, -0.520°, 0.340°, -0.442°].

The joint torques and power required for tracking the input trajectories are shown in Fig. 12. Based on Fig. 12 it is also shown that the peak torque and power required for simultaneous trajectory tracking are [-73.83, 156.71, -77.29, 4.01, 6.08, 0.41] Nm and [-65.40, -189.21, 44.19, 94.57, 7.53, 0.09] Watts.

The total power consumed by all 7 joints and the peak power required is shown in Fig. 13. The friction torque developed during trajectory tracking is given in Fig. 14.

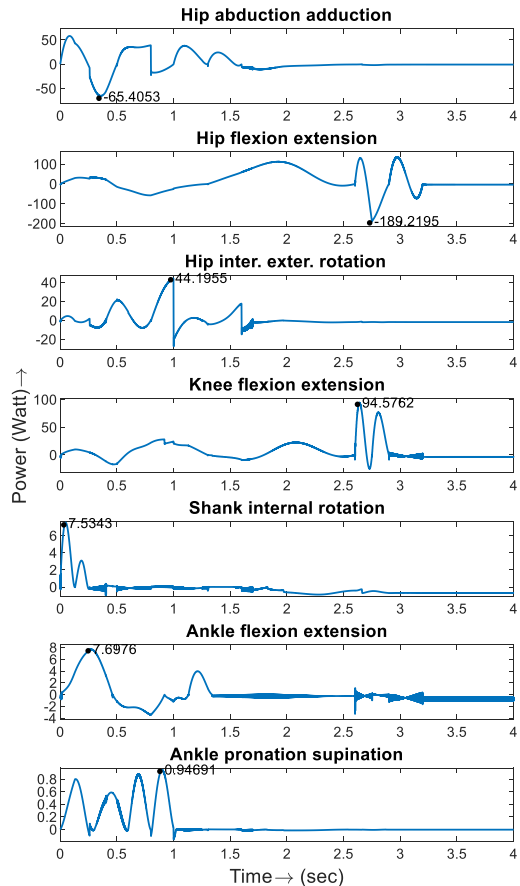


**Fig. 12:** Joint torque and power used during trajectory tracking using LQR

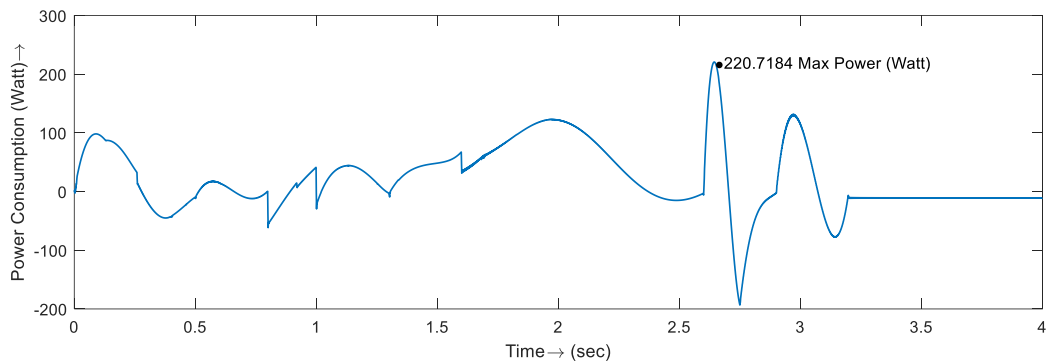


**Fig. 13:** Total power consumed by all seven joints during simultaneous trajectory tracking using LQR

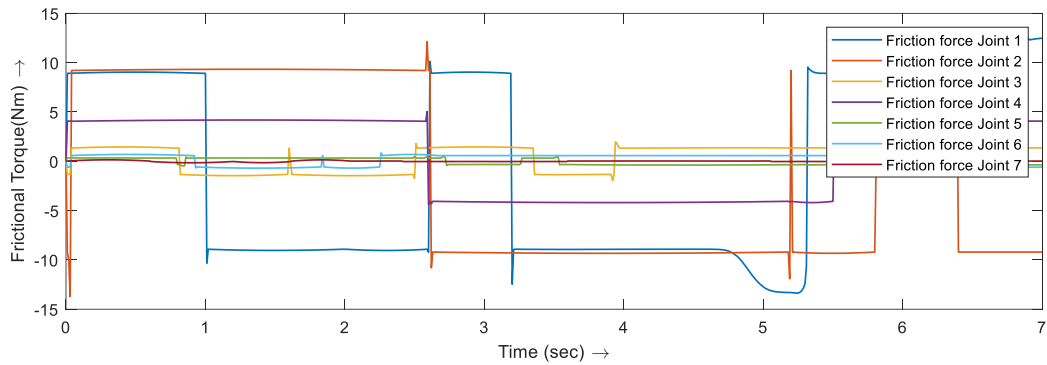


**Fig. 14:** Friction force developed during simultaneous joint movement using LQR

**Table 5:** Comparison between LQR and PID, CTC and SMC performance

Control scheme	Joint #	Max. tracking error ( $^{\circ}$ )	Peak torque (Nm)	Peak power (Watt)	Combined peak power (Watt)	Total energy consumption (Joule)
LQR controller	Joint 1	0.370	73.8320	65.405	217.690	$8.763 \times 10^1$
	Joint 2	0.085	156.7160	189.219		
	Joint 3	0.396	17.1090	44.195		
	Joint 4	0.199	77.2940	94.576		
	Joint 5	0.520	4.0110	7.534		
	Joint 6	0.340	6.0860	7.697		
	Joint 7	0.442	0.4100	0.947		
Sliding mode controller	Joint 1	0.808	69.5830	88.727	218.833	$2.011 \times 10^2$
	Joint 2	0.128	152.7190	215.516		
	Joint 3	0.824	16.7090	42.419		
	Joint 4	0.577	67.6150	91.368		
	Joint 5	1.279	4.1400	7.674		
	Joint 6	0.730	6.6840	6.931		
	Joint 7	0.616	0.4191	0.981		
Computed torque controller	Joint 1	0.067	80.0300	112.400	393.302	$1.465 \times 10^2$
	Joint 2	0.097	261.7000	316.700		
	Joint 3	0.093	26.9400	38.780		
	Joint 4	0.247	59.5500	90.250		
	Joint 5	0.453	11.6300	11.080		
	Joint 6	0.331	8.9050	12.410		
	Joint 7	1.563	1.2400	3.534		
PID controller	Joint 1	0.042	127.0000	103.400	276.400	$4.361 \times 10^2$
	Joint 2	0.028	290.6000	209.500		
	Joint 3	0.008	18.3600	12.820		
	Joint 4	0.093	44.6800	26.060		
	Joint 5	0.000	14.7600	3.215		
	Joint 6	0.003	7.6900	3.244		
	Joint 7	0.000	2.1900	1.043		

## Comparison between LQR and other Control Schemes

The trajectory tracking performance of the proposed LQR is compared to PID, Computed Torque Controller (CTC), and Sliding Mode Controller (SMC) to evaluate its effectiveness. A more detailed description of CTC, PID, and SMC is available (Hasan and Dhingra, 2021). Table 5 shows the joint-wise maximum trajectory tracking errors, peak torque requirements (Nm), peak power requirements, combined peak power requirement, and the total energy consumption. For evaluating the trajectory tracking performance, the same dynamic model and same input trajectories are used.

It has been noticed that for tracking the same trajectories, the LQR required the minimum combined peak power (217.69 Watts) and the energy (87.63 Joules). The PID controller offered the best trajectory tracking accuracy but required significantly high joint torques and total energy.

## Conclusion

A 7-DoF human lower extremity kinematic and dynamic model was developed using the Newton Euler method. A linearized state-space model of the robot was presented. A linear quadratic regulator was designed and its performance was assessed by dynamic simulation. To replicate an actual robot, a realistic friction model was developed and used. The LQR showed superior trajectory tracking performance. The stability analysis of the developed controller was presented. For performance evaluation, the trajectory tracking the performance of the LQR scheme is compared with PID, CTC, and SMC methods. It has been noticed that by using LQR, the trajectory tracking errors are within the acceptable range ( $1^\circ$  or less) and the LQR controller required significantly lower joint torque and total energy compared to the other three controllers.

Future work will include designing a human rehabilitating exoskeleton robot for the human lower extremities and the realization of the proposed LQR for controlling the lower extremity rehabilitation exoskeleton robot.

## Author's Contributions

**SK Khairul Hasan:** Concept development, dynamic modeling, Simulation, organization and writing.

**Anoop Dhingra:** Proof-reading and editing the manuscript.

## Ethics

This article is original and contains unpublished material. Authors declare that are no ethical issues and no conflict of interest may arise after the publication of this manuscript.

## Reference

- Agrawal, S. K., Banala, S. K., Fattah, A., Sangwan, V., Krishnamoorthy, V., Scholz, J. P., & Hsu, W. L. (2007). Assessment of motion of a swing leg and gait rehabilitation with a gravity balancing exoskeleton. *IEEE Transactions on Neural Systems and Rehabilitation Engineering*, 15(3), 410-420. doi.org/10.1109/TNSRE.2007.903930
- Araujo, M. V., Alsina, P. J., Roza, V. C. C., & Melo, N. B. (2015). Powered orthosis ortholeg: Design and development. *IEEE Latin America Transactions*, 13(1), 90-95. doi.org/10.1109/TLA.2015.7040633
- Banala, S. K., Agrawal, S. K., & Scholz, J. P. (2007, June). Active Leg Exoskeleton (ALEX) for gait rehabilitation of motor-impaired patients. In 2007 IEEE 10th international conference on rehabilitation robotics (pp. 401-407). IEEE. doi.org/10.1109/ICORR.2007.4428456
- Bernhardt, M., Frey, M., Colombo, G., & Riener, R. (2005, June). Hybrid force-position control yields cooperative behavior of the rehabilitation robot LOKOMAT. In 9th International Conference on Rehabilitation Robotics, 2005. ICORR 2005. (pp. 536-539). IEEE. https://ieeexplore.ieee.org/abstract/document/1501159
- Chen, B., Zhong, C. H., Zhao, X., Ma, H., Guan, X., Li, X., ... & Liao, W. H. (2017). A wearable exoskeleton suit for motion assistance to paralyzed patients. *Journal of orthopedic translation*, 11, 7-18. doi.org/10.1016/j.jot.2017.02.007
- Chen, B., Zhong, C. H., Zhao, X., Ma, H., Qin, L., & Liao, W. H. (2019). Reference joint trajectories generation of CUHK-EXO exoskeleton for system balance in walking assistance. *IEEE Access*, 7, 33809-33821. doi.org/10.1109/ACCESS.2019.2904296
- Colombo, G., Joerg, M., Schreier, R., & Dietz, V. (2000). Treadmill training of paraplegic patients using a robotic orthosis. *Journal of rehabilitation research and development*, 37(6), 693-700.
- Contini, R. (1972). Body segment parameters, Part II. *Artificial limbs*, 16(1), 1-19. http://oandplibrary.org/al/pdf/1972\_01.pdf#page=5
- Craig, J. J. (2005). Introduction to robotics: Mechanics and control. Pearson Educacion. ISBN-10: 9702607728.
- Engin, M. (2018, June). Embedded LQR controller design for self-balancing robot. In 2018 7th Mediterranean Conference on Embedded Computing (MECO) (pp. 1-4). IEEE. doi.org/10.1109/MECO.2018.8405959
- Esquenazi, A., Talaty, M., Packel, A., & Saulino, M. (2012). The ReWalk powered exoskeleton to restore ambulatory function to individuals with thoracic-level motor-complete spinal cord injury. *American journal of physical medicine & rehabilitation*, 91(11), 911-921. doi.org/10.1097/PHM.0b013e318269d9a3

- Farris, R. J., Quintero, H. A., Murray, S. A., Ha, K. H., Hartigan, C., & Goldfarb, M. (2013). A preliminary assessment of legged mobility provided by a lower limb exoskeleton for persons with paraplegia. *IEEE Transactions on neural systems and rehabilitation engineering*, 22(3), 482-490. doi.org/10.1109/TNSRE.2013.2268320
- Gloster, M., Alsina, P. J., & Melo, N. B. (2015, November). Ortholeg 2.0-a new design for a lower limb active orthosis. In 2015 International symposium on micro-nanomechatronics and human science (MHS) (pp. 1-7). IEEE. doi.org/10.1109/MHS.2015.7438347
- Ha, J. L., Fung, R. F., Han, C. F., & Chang, J. R. (2006). Effects of frictional models on the dynamic response of the impact drive mechanism. doi.org/10.1115/1.2128641
- Hasan, S. K., & Dhingra, A. K. (2020). 8 Degrees of freedom human lower extremity kinematic and dynamic model development and control for exoskeleton robot based physical therapy. *International Journal of Dynamics and Control*, 8(3), 867-886. doi.org/10.1007/s40435-020-00620-3
- Hasan, S. K., & Dhingra, A. K. (2021). Performance verification of different control schemes in human lower extremity rehabilitation robot. *Results in Control and Optimization*, 4, 100028. doi.org/10.1016/j.rico.2021.100028
- Hazem, Z. B., Fotuhi, M. J., & Bingül, Z. (2020). Development of a Fuzzy-LQR and Fuzzy-LQG stability control for a double link rotary inverted pendulum. *Journal of the Franklin Institute*, 357(15), 10529-10556. doi.org/10.1016/j.jfranklin.2020.08.030
- Jianfeng, S., Runze, Y., & Linhong, J. (2013). Lower-limb robot-assisted therapy in rehabilitation of acute and subacute stroke patients. In World Congress on Medical Physics and Biomedical Engineering May 26-31, 2012, Beijing, China (pp. 2034-2037). Springer, Berlin, Heidelberg. doi.org/10.1007/978-3-642-29305-4\_534
- Kawamoto, H., & Sankai, Y. (2004, September). Power assist method based on phase sequence driven by interaction between human and robot suit. In ROMAN 2004. 13th IEEE International Workshop on Robot and Human Interactive Communication (IEEE Catalog No. 04TH8759) (pp. 491-496). IEEE. https://ieeexplore.ieee.org/abstract/document/1374809
- Kawamoto, H., Hayashi, T., Sakurai, T., Eguchi, K., & Sankai, Y. (2009, September). Development of single leg version of HAL for hemiplegia. In 2009 Annual international conference of the IEEE engineering in medicine and biology society (pp. 5038-5043). IEEE. doi.org/10.1109/EMBS.2009.5333698
- Kazerooni, H., Steger, R., & Huang, L. (2006). Hybrid control of the Berkeley lower extremity exoskeleton (BLEEX). *The International Journal of Robotics Research*, 25(5-6), 561-573. doi.org/10.1177/0278364906065505
- Kendall, F. P., McCreary, E. K., Provance, P. G., Rodgers, M. M., & Romani, W. A. (2005). Muscles: Testing and function with posture and pain (Vol. 5, pp. 1-100). Baltimore, MD: Lippincott Williams & Wilkins. https://www.oandp.org/page/BookRev\_FPeterson
- Kim, J. H., Han, J. W., Kim, D. Y., & Baek, Y. S. (2013). Design of a walking assistance lower limb exoskeleton for paraplegic patients and hardware validation using CoP. *International Journal of Advanced Robotic Systems*, 10(2), 113. doi.org/10.5772/55336
- Kim, S.H., (2010) Robot-assisted modifications of gait in healthy individuals. *Experimental Brain Research*, 2010. 202(4): p. 809-824. doi.org/10.1007/s00221-010-2238-y
- Kurz, T. (2015). Normal Ranges of Joint Motion. 2015; http://web.mit.edu/tkd/stretch/stretching\_8.html
- Kwa, H. K., Noorden, J. H., Missel, M., Craig, T., Pratt, J. E., & Neuhaus, P. D. (2009, May). Development of the IHMC mobility assist exoskeleton. In 2009 IEEE international conference on robotics and automation (pp. 2556-2562). IEEE. doi.org/10.1109/ROBOT.2009.5152394
- Liu, S., & Chen, G. S. (2019). Dynamics and control of robotic manipulators with contact and friction. John Wiley & Sons. doi.org/10.1002/9781119422518
- Marcheschi, S., Salsedo, F., Fontana, M., & Bergamasco, M. (2011, May). Body extender: whole body exoskeleton for human power augmentation. In 2011 IEEE international conference on robotics and automation (pp. 611-616). IEEE. doi.org/10.1109/ICRA.2011.5980132
- Meng, W., Liu, Q., Zhou, Z., Ai, Q., Sheng, B., & Xie, S. S. (2015). Recent development of mechanisms and control strategies for robot-assisted lower limb rehabilitation. *Mechatronics*, 31, 132-145. doi.org/10.1016/j.mechatronics.2015.04.005
- Morales, S., Magallanes, J., Delgado, C., & Canahuire, R. (2018, November). LQR trajectory tracking control of an omnidirectional wheeled mobile robot. In 2018 IEEE 2nd Colombian Conference on Robotics and Automation (CCRA) (pp. 1-5). IEEE. doi.org/10.1109/CCRA.2018.8588146
- Mori, Y., Okada, J., & Takayama, K. (2006). Development of a standing style transfer system "ABLE" for disabled lower limbs. *IEEE/ASME Transactions on Mechatronics*, 11(4), 372-380. doi.org/10.1109/TMECH.2006.878558

- Neuhaus, P. D., Noorden, J. H., Craig, T. J., Torres, T., Kirschbaum, J., & Pratt, J. E. (2011, June). Design and evaluation of Mina: A robotic orthosis for paraplegics. In 2011 IEEE international conference on rehabilitation robotics (pp. 1-8). IEEE.  
[doi.org/10.1109/ICORR.2011.5975468](https://doi.org/10.1109/ICORR.2011.5975468)
- Nikolova, G., & Toshev, Y. (2008). Comparison of two approaches for calculation of the geometric and inertial characteristics of the human body of the Bulgarian population. *Acta of bioengineering and biomechanics*, 10(1), 3.  
<http://citeseerx.ist.psu.edu/viewdoc/download?doi=10.1.1.1084.477&rep=rep1&type=pdf>
- Ortega-Vidal, A., Salazar-Vasquez, F., & Rojas-Moreno, A. (2020, September). A comparison between optimal LQR control and LQR predictive control of a planar robot of 2DOF. In 2020 IEEE XXVII International Conference on Electronics, Electrical Engineering and Computing (INTERCON) (pp. 1-4). IEEE.  
[doi.org/10.1109/INTERCON50315.2020.9220263](https://doi.org/10.1109/INTERCON50315.2020.9220263)
- Russell, F., Vaidyanathan, R., & Ellison, P. (2018, August). A kinematic model for the design of a bicondylar mechanical knee. In 2018 7th IEEE international conference on biomedical robotics and biomechatronics (Biorob) (pp. 750-755). IEEE.  
[doi.org/10.1109/BIOROB.2018.8487734](https://doi.org/10.1109/BIOROB.2018.8487734)
- Sanz-Merodio, D., Cestari, M., Arevalo, J. C., & Garcia, E. (2012). Control motion approach of a lower limb orthosis to reduce energy consumption. *International journal of advanced robotic systems*, 9(6), 232.  
[doi.org/10.5772/51903](https://doi.org/10.5772/51903)
- Schoenwald, D. A., Feddema, J. T., Eisler, G. R., & Segalman, D. J. (1990). Minimum-time trajectory control of a two-link flexible robotic manipulator (No. SAND-90-2472C; CONF-910451-10). Sandia National Labs., Albuquerque, NM (USA).
- Singh, N., Sharma, R., & Rekhi, N. S. (2010). LQR Controller for Two Link Rigid Manipulator. 2010.
- Stegall, P., K.N. Winfree and S.K. Agrawal. Degrees-of-freedom of a robotic exoskeleton and human adaptation to new gait templates. in 2012 IEEE International Conference on Robotics and Automation. 2012.  
[doi.org/10.1109/ICRA.2012.6225092](https://doi.org/10.1109/ICRA.2012.6225092)
- Strickland, E. (2011). Good-bye, Wheelchair, Hello Exoskeleton. 2011.  
<http://spectrum.ieee.org/biomedical/bionics/goodbye-wheelchair-hello-exoskeleton>
- Surgeons., A. A. O. O. (1965). Joint Motion: Methods of Measuring and Recording. 1965: Chicago: American Academy of Orthopaedic Surgeons.
- Suzuki, K., Mito, G., Kawamoto, H., Hasegawa, Y., & Sankai, Y. (2007). Intention-based walking support for paraplegia patients with Robot Suit HAL. *Advanced Robotics*, 21(12), 1441-1469.  
<https://www.tandfonline.com/doi/abs/10.1163/156855307781746061>
- Tagliamonte, N. L., Sergi, F., Carpino, G., Accoto, D., & Guglielmelli, E. (2013, June). Human-robot interaction tests on a novel robot for gait assistance. In 2013 IEEE 13th international conference on rehabilitation robotics (ICORR) (pp. 1-6). IEEE.  
[doi.org/10.1109/ICORR.2013.6650387](https://doi.org/10.1109/ICORR.2013.6650387)
- Veneman, J. F., Ekkelenkamp, R., Kruidhof, R., van der Helm, F. C., & van der Kooij, H. (2006). A series elastic-and bowden-cable-based actuation system for use as torque actuator in exoskeleton-type robots. *The international journal of robotics research*, 25(3), 261-281.  
<https://journals.sagepub.com/doi/abs/10.1177/0278364906063829>
- Veneman, J. F., Kruidhof, R., Hekman, E. E., Ekkelenkamp, R., Van Asseldonk, E. H., & Van Der Kooij, H. (2007). Design and evaluation of the LOPES exoskeleton robot for interactive gait rehabilitation. *IEEE Transactions on Neural Systems and Rehabilitation Engineering*, 15(3), 379-386.  
[doi.org/10.1109/TNSRE.2007.903919](https://doi.org/10.1109/TNSRE.2007.903919)
- Wang, L., Wang, S., van Asseldonk, E. H., & van der Kooij, H. (2013, November). Actively controlled lateral gait assistance in a lower limb exoskeleton. In 2013 IEEE/RSJ International Conference on Intelligent Robots and Systems (pp. 965-970). IEEE.
- Wei, L., & Yao, W. (2015, August). Design and implement of LQR controller for a self-balancing unicycle robot. In 2015 ieee international conference on information and automation (pp. 169-173). IEEE.  
[doi.org/10.1109/ICInfA.2015.7279279](https://doi.org/10.1109/ICInfA.2015.7279279)
- Yamamoto, K., Ishii, M., Noborisaka, H., & Hyodo, K. (2004, September). Stand alone wearable power assisting suit-sensing and control systems. In RO-MAN 2004. 13th IEEE International Workshop on Robot and Human Interactive Communication (IEEE Catalog No. 04TH8759) (pp. 661-666). IEEE.  
<https://ieeexplore.ieee.org/abstract/document/1374841/>
- Yan, T., Cempini, M., Oddo, C. M., & Vitiello, N. (2015). Review of assistive strategies in powered lower-limb orthoses and exoskeletons. *Robotics and Autonomous Systems*, 64, 120-136.  
[doi.org/10.1016/j.robot.2014.09.032](https://doi.org/10.1016/j.robot.2014.09.032)
- Yang, S., Han, J., Xia, L., & Chen, Y. H. (2020). An optimal fuzzy-theoretic setting of adaptive robust control design for a lower limb exoskeleton robot system. *Mechanical Systems and Signal Processing*, 141, 106706. doi.org/10.1016/j.ymssp.2020.106706

- Yoshimitsu, T., & Yamamoto, K. (2004, August). Development of a power assist suit for nursing work. In SICE 2004 annual conference (Vol. 1, pp. 577-580). IEEE.
- Zelig, G., Weingarten, H., Zwecker, M., Dudkiewicz, I., Bloch, A., & Esquenazi, A. (2012). Safety and tolerance of the ReWalk™ exoskeleton suit for ambulation by people with complete spinal cord injury: A pilot study. *The journal of spinal cord medicine*, 35(2), 96-101. doi.org/10.1179/2045772312Y.0000000003
- Zhao, J., & Ruan, X. (2008). The LQR control and design of dual-wheel upright self-balance robot. *Intelligent Control and Automation*, 4864-4869.  
doi.org/10.1109/WCICA.2008.4593712
- Zoss, A. B., Kazerooni, H., & Chu, A. (2006). Biomechanical design of the Berkeley Lower Extremity Exoskeleton (BLEEX). *IEEE/ASME Transactions on mechatronics*, 11(2), 128-138. doi.org/10.1109/TMECH.2006.871087